

Experimental investigation of turbulent density fluctuations and noise generation from heated jets

J. PANDA

Ohio Aerospace Institute and NASA Glenn Research Center, Brookpark, OH 44135, USA

(Received 13 July 2005 and in revised form 26 April 2007)

Low-frequency noise sources in heated single-stream jets were identified by cross-correlating turbulent density fluctuations ρ' with the far-field sound pressure fluctuations p' . The turbulent density fluctuations were measured by a molecular Rayleigh-scattering technique. For a fixed jet velocity U_j , the normalized correlation coefficient $\langle \rho'; p' \rangle / (\rho'_{rms} p'_{rms})$ is found to increase progressively with an increase in the plume temperature (subscript *rms* stands for root-mean-square). The result indicates an improvement of the noise radiation efficiency with heating. Directly measured noise spectra from fixed velocity jets with increasing temperature ratio show confusing trends. However, if such spectra are normalized by the plume density, then a consistent trend of increasing noise level with increased plume temperature emerges. The increased noise is the most prominent at the low-frequency end, consistent with the correlation data. The effect of increasing jet velocity keeping the plume temperature constant was also studied. The correlation coefficients were found to improve significantly with velocity; a result consistent with prior observation from unheated jets. Additional findings on the time-averaged density variations and the changes in the air density fluctuations with increasing plume temperature are also discussed.

1. Introduction

The noise emitted by the exhaust plume from a gas turbine engine continues to be a significant contributor to the total amount of noise radiation from current commercial airplanes. As community standards lower the acceptable noise thresholds, noise abatement issues are gaining prominence in engine design. There is a continuing need to further understand the noise generation mechanisms and to develop noise reduction technologies. Such technologies are expected to have significant economical impacts. One of the important issues in both the physical understanding and the modelling of noise sources has been the effect of varying plume temperature on noise radiation. The problem is an old one and there are many past experimental efforts to characterize the changes (Hoch *et al.* 1973; Tanna, Dean & Burrin 1976; Tanna 1977; Bridges & Wernet 2003; Viswanathan 2004, 2006). Except for Bridges & Wernet, all of these works exclusively looked into the far-field noise spectra and documented the changes associated with increased plume temperature. Bridges & Wernet (2003) used particle image velocimetry to determine changes in turbulent scales with heating. The motivation for the present work comes from the recent advances in molecular Rayleigh-scattering-based instrumentation to measure turbulence fluctuations in high velocity and heated flows. We have published two noise source studies from unheated jets (Panda & Seasholtz 2002; Panda, Seasholtz & Elam 2005, hereinafter referred to

as PS and PSE, respectively), where fluctuations in turbulent density ρ and momentum fluxes ρuu , ρvv (u is the axial component of velocity, v is the radial component) were correlated separately with far-field sound pressure fluctuations. The present work is an extension for heated jets. The goal is to measure the changes in turbulent fluctuations and noise sources that accompany an increase in the plume temperature.

The source of the jet noise is the turbulent fluctuations in the plume; and like turbulence there exist multiple, and sometimes contradictory, descriptions of the noise source. Morfey (1973) gave the first analytical description of the additional noise source created by heating. He showed that heated jets have a dipole noise source term, in addition to the quadrupole term present in the unheated counterpart. The former scales to the sixth power of velocity compared to the eighth power for the latter. A number of other analytical works followed (Morfey, Szewczyk & Tester 1978; Fisher, Lush & Harper-Bourne 1973, among others). Michalke & Michel (1979) showed that the quadrupole source term can be described as the second time derivative of a source quantity q_1 , which is primarily a product of density and the square of the component of the velocity fluctuations directed toward the observer. The dipole source term is derived as the first time derivative of q_2 , which is the product of the local pressure and the gradient of the ratio between ambient and local densities toward the observer. Therefore, a change of density modifies both source terms: the quadrupole and the dipole. Most of these analytical works stem from a need to explain the experimentally observed deviation from the u^8 scaling law for the far-field noise spectra measured from low-speed heated jets. However, the quality of these experimental data has remained questionable since the early days. Low-velocity noise data are expected to be contaminated by facility-related spurious noise. Most workers have acknowledged this and endeavored to minimize contamination. Viswanathan (2004) has argued that the additional features in the noise spectrum supporting the presence of the second noise source are entirely due to the spurious facility noise.

Advancements in the computational aeroacoustics have allowed for an in-depth investigation into noise sources. Freund (2002) calculated contributions to far-field noise from various components of the noise source tensor using direct numerical simulation (DNS) of a low-Reynolds-number jet. He found that the components were so interrelated that the contribution from one cancels that from the other. Therefore, efforts to isolate the contribution from the pressure-density term from that of the fluctuating momentum flux term, solely based upon the far-field noise spectra, are misguided. All of these demonstrate pitfalls in creating models based only on the far-field noise measurements.

It is believed that continuing advancements in experimental techniques and numerical simulations will provide better insights into the turbulent structures and interactions leading to noise generation. Tam, Golebiowski & Seiner (1996) has proposed a two-scale (large-scale and fine-scale) model based on the structural description of turbulence. The energy-containing low-frequency part of the turbulent fluctuations is expected to produce the shallow angle 'large-scale' part of the noise, whereas the smaller eddies produce omni-directive fine-scale noise. The latter was modelled by Tam & Auriult (1999). Viswanathan (2004) used the empirical formulation generated from this two-scale model to discredit the dipole noise source formulations as discussed above. Recent insights obtained from DNS and large-eddy simulations (LES) are examples of associating noise generation with the details of turbulence events. Bogey & Bailly (2005) demonstrated success in reproducing the flow-sound correlation results via LES of jet flows. They were able to reproduce various trends reported in our prior experimental work. The LES database also

M_a	T_r	Plenum T (K)	M_j	U_j (m s^{-1})	ρ_j/ρ_a	$Re \times 10^6$	Specific heat ratio γ	Tanna point
0.90	0.840	289	0.982	306	1.19	1.41	1.3999	7
0.90	1.000	335	0.900	306	1.00	1.03	1.3995	12
0.90	1.429	458	0.754	306	0.70	0.55	1.3947	19
0.90	1.818	569	0.671	306	0.55	0.37	1.3845	27
0.90	2.273	699	0.604	306	0.44	0.25	1.3690	36
0.90	2.700	821	0.557	306	0.37	0.19	1.3550	46*
0.60	2.273	675	0.402	204	0.44	0.17	1.3690	33
1.48	2.273	772	0.993	504	0.44	0.42	1.3690	39
1.48	2.700	893	0.916	504	0.37	0.32	1.3550	49*

* Higher temperature ratio (2.86) used by Tanna *et al.* (1976).

TABLE 1. Operating conditions.

allowed for an in-depth look into turbulence parameters, such as the vorticity fluctuations, which are difficult to measure experimentally. They noticed significant intermittency in the vorticity fluctuations at the end of the potential core and have associated intermittent intrusion of the vortical structures into the jet core as the events responsible for the low-frequency noise generation. All of these point out the advancements in noise source identification achievable by turbulence investigations.

The turbulent mixing behaviour of heated jets was the subject of many experimental and analytical papers. Monkewitz *et al.* (1990), Russ & Strykowski (1993), Hugo & McMackin (1997) looked into the onset of absolute instability and the behaviour of the Kelvin–Helmholtz instability in heated jets. Such studies were mostly performed in low-velocity jets; and the appearance of the absolute instability in high-velocity jets is yet to be confirmed. Ötügen & Namer (1988) used a Rayleigh-scattering technique to measure time-average density which was then used to calculate the local temperature, assuming constant static pressure. Doty & McLaughlin (2003) report an increased spreading rate with increasing helium injection from a simulated heated-jet study. The present work is centred on the unsteady density fluctuations in high-speed heated plumes. Section 2 describes the Rayleigh-scattering set-up. Section 3 describes the changes in time-averaged density, standard deviation of density fluctuations, and density fluctuation spectrum that occur with increased plume temperature and velocity. Section 4 provides changes in correlation between near-field and far-field fluctuations. The last part analyses the far-field noise spectra and provides evidence supporting observations made in the flow–sound correlation study.

2. Experimental set-up

The experiment was performed in the small hot jet acoustic rig in the Aeroacoustics Propulsion Laboratory (AAPL) of NASA Glenn Research Center (Bridges & Brown 2005). The jet facility is capable of producing heated jets with total temperature from ambient to 920 K (1650 R) in the aerodynamic Mach number range $0 < M_j < 2$, and therefore ideal for studying the effect of heating. A 50.8 mm (2 in) diameter convergent nozzle was used for all measurement conditions. The operating conditions are shown in table 1 and presented in figure 1. The choice of operating conditions is guided by the work of Tanna (1977) and Tanna *et al.* (1976) whose far-field noise database was used in the earlier plots. Bridges & Wernet (2003) have reported time average velocity and turbulent kinetic energy data from PIV tests on the same jets. The test conditions were

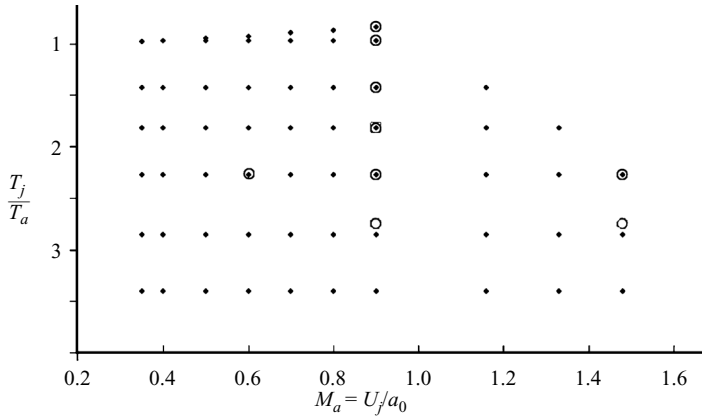


FIGURE 1. Jet operating conditions. The points are subsonic conditions used by Tanna *et al.* (1976) for a shock-free convergent nozzle and the circles are the Rayleigh test points.

chosen such that one set of points reflects the effect of static temperature variation for a constant $M_a = 0.9$, and the second set reflects the effect of jet velocity for constant temperature ratio $T_r = 2.27$. Similarly to Tanna *et al.* (1976), acoustic Mach number $M_a (=U_j/a_a$, where U_j is the velocity inside the jet core and a_a is the ambient speed of sound), as opposed to the aerodynamic Mach number $M_j (=U_j/a_j$, where a_j is the sound speed in the jet core), and jet static temperature ratio $T_r (=$ core static temperature T_j /ambient temperature T_a) as opposed to a ratio of total temperature are used in the present work. Increasing plume temperature is associated with a reduction of the aerodynamic Mach number and Reynolds number. While M_a is the commonly used parameter for sound radiation (that involves coupling between jet velocity and ambient sound speed), the compressibility effect is represented by the aerodynamic Mach number M_j . To fix acoustic Mach number, the aerodynamic Mach number has to be lowered for higher-temperature plumes. The other effect of heating is a significant reduction in Reynolds number. In the past, the lowering of the Reynolds number has been suspected to relaminarize the initial lip shear layer, leading to changes in noise sources.

The far-field sound pressure fluctuations were measured by an array of seven $1/4$ in (6.35 mm) microphones kept on an arc of $100D$ (5.08 m) and centred at the nozzle exit. The microphones were angularly placed with 10° increments: from 150° to 90° to the jet exit. (In PS and PSE, microphone polar angles were measured from the jet-flow direction, whereas here polar angles are presented from the flight direction. While the former is better suited for spherical coordinate specification of noise radiation, the latter is more commonly used in the aircraft community. Nonetheless, 150° in the present paper is equivalent to 30° in the earlier.) The presence of the large traversing unit, optical components and other metal surfaces was a concern for significant acoustic reflection. To minimize such reflection a large part of such surfaces were covered by 50 mm thick polyurethane foam.

2.1. Rayleigh set-up

Although Rayleigh scattering can be used to measure temperature, density and velocity simultaneously, it was decided to resort to a set-up for density only in this first attempt on a heated-jet facility. Once density measurement becomes feasible by mitigating various issues with particle removal and vibration isolation, velocity and

temperature measurements are possible via optical spectral analysis of the collected scattered light.

The principle for air density measurement using Rayleigh scattering has been discussed in PS and Panda *et al.* (2004). In brief, for a fixed composition of gas (fixed Rayleigh-scattering cross-section) and fixed optical set-up, the Rayleigh-scattered light intensity is directly proportional to the molecular number density and, in turn, to bulk density ρ . Photomultiplier tubes and photon counting electronics were used to measure the scattered power. The number of photo-electrons N arriving over a time interval Δt is directly proportional to the scattered light intensity and therefore, to the bulk density ρ :

$$N = k''\rho \Delta t \quad (k'' = \text{constant}). \quad (1)$$

In reality, the Rayleigh-scattered light is contaminated by a small amount of background light. Therefore, the linear relation has two constants k and k' to be determined via calibration in known density flows:

$$N = (k\rho + k') \Delta t. \quad (2)$$

Since scattering from the dust particles can easily overwhelm the Rayleigh signature, soot generation from the combustors was another concern. To avoid soot, a hydrogen combustor was used. Burning hydrogen produced steam, which did not condense in the high-temperature plume. Note that the Rayleigh-scattering cross-section of steam is 13 % lower than that of oxygen. Since the combustion process replaced some oxygen by steam, the Rayleigh-scattering cross-section for the heated air is expected to be different from the ambient. The difference, however, is calculated to be small ($\sim 0.5\%$) even for the maximum jet temperature. No special steps were taken to account for this difference which has manifested as a source of measurement uncertainty. Another potentially significant problem in Rayleigh set-ups is moisture condensation. For the present set-up, the condensation was absent whenever the combustor was used. Unheated jets in Mach number $M_a \geq 0.9$ showed a trace of fogging which prohibited detailed survey of these jets.

The Rayleigh set-up was built in two parts (figure 2): the first is around the jet facility and the second part inside a control room away from the facility. Dry compressed air was supplied to the facility from a central air handler. The compressed air was passed through additional $0.3\ \mu\text{m}$ filters for dust removal. Just before the test, the facility was used for particle image velocimetry (PIV) study. The interior of a significant part of the facility, from settling chamber to the nozzle lip, was covered by a thick layer of aluminium oxide powder. All components were dismantled, cleaned and reassembled before the test. The seed particles create a general nuisance as every surface of the anechoic chamber and all sound absorbing wedges are covered by the particles. The cleaning part was confined to the interior flow passage of the primary jet. Additionally, the jet was surrounded by a clean co-flow stream from a $280\ \text{mm} \times 280\ \text{mm}$ square opening. The co-flow was created by a separate air blower that took in the ambient air and passed it through a $0.3\ \mu\text{m}$ filter. The filtered air was passed to a settling chamber built around the outside of the facility and finally exhausted through the square opening at a speed of around $20\ \text{m s}^{-1}$. A round co-flow would have been more suitable for the round nozzles used in this study; however, the square duct was readily available and served the purpose.

Similarly to the earlier efforts on unheated jets (PS), the present set-up was for a point measurement technique. A continuous-wave laser beam was passed normal to the jet axis and the light scattered from a small region on the beam was collected and

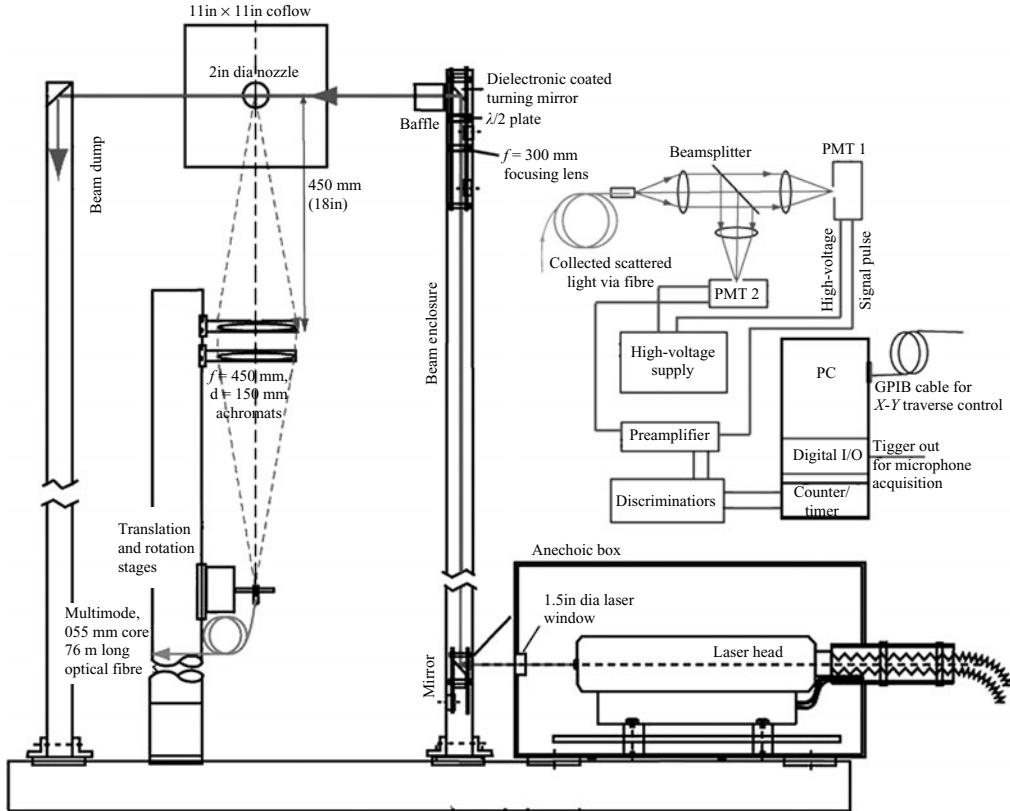


FIGURE 2. A schematic of the Rayleigh set-up.

focused onto an optical fibre. The part of the set-up, around the jet facility, was built on a large 2-axis (axial x and radial r) traversing unit that allowed plume survey in one (x, r) -plane. The light source was a solid-state frequency doubled Nd:VO₄ laser that produced 5 W power at 532 nm wavelength. The laser head was also mounted on the traverse. To avoid damage from the high noise level produced by the jets, the laser head was enclosed in an anechoic box (figures 2). The incident laser beam was focused at the probe volume by a 500 mm focal length achromat and the polarization was adjusted for maximum scattering intensity towards the 90°, vertically down, collection direction. The beam, after crossing the plume, was dissipated in a long and narrow dump. The collection lens consisted of a pair of $f/3$, 150 mm diameter achromats that focused the collected light on a 550 μm multimode optical fibre. The combination of the fibre diameter and 1:1 imaging fixed the measurement probe volume length to 550 μm . The beam waist was about 150 μm in diameter. Since stray scattering of the incident beam can overwhelm the Rayleigh signal, various baffles were created in the transmission path. Except for the portion of the beam that crossed the jet, the laser path was covered with metal tubes. To avoid collection of stray background light, the collection lenses were placed in an enclosure with one end open towards the beam, and a large 380 mm diameter hollow tube, suspended from the top, provided a dark background (Panda *et al.* 2004). Additionally, to avoid sunlight, the entire test was conducted after dark: between 10:30 p.m. and 6 a.m.

The 76 m long optical fibre passed the collected scattered light to a control room for light intensity measurement. Here, the collected light was collimated and then split into two equal parts by a beam splitter. Each of the beams was refocused into individual photomultiplier tubes (PMT). The purpose of two photomultipliers is to reduce the effect of electronic shot noise in density spectrum calculations (PS). Photon-counting electronics were used to measure light intensities. Each PMT channel terminated in a pre-amplifier and passed to constant-fraction discriminators, and finally to a multi-channel timer-counter board. The counting was performed over a series of contiguous time bins of 10 to 20 μs time interval. Usually a million contiguous bins were used to obtain long time-series data. Before processing, the counts in every bin were corrected for the pulse pile-up error. The entire data-collection process was automated to move the laser probe volume from point to point in the flow field, perform the photon-counting process and collect the time histories.

The following is a comment on the uncertainty in the laser probe location. The traversing system was found to travel at a small angle with respect to the jet centreline. At a downstream distance of two jet diameters, the laser probe was at the centreline; however, at $x/D = 10$, the probe moved to approximately $r/D = 0.1$. The time-averaged profiles presented in this paper were corrected for this slant. However, the correlation data are presented with the radial location as measured.

The microphone time signals were acquired by a separate processing and data acquisition system. For correlating the density fluctuations to the far-field noise signal, the photo-electron counting and the digitization of the microphone signals had to be synchronized. This was a two-step process. First, the timer-counter board for the photo-electron counting was operated from the clock pulses produced by the microphone data acquisition system. Secondly, a single pulse from a separate digital input/output generator initiated both counting and digitization processes. To verify time synchronization, a synthetic signal was measured and compared. The synthetic signal was digitized by the microphone signal processor and also used to drive a light emitting diode (LED). The LED produced light intensity modulation at the synthetic signal frequency and was placed in front of a PMT. Finally, the above data acquisition electronics were used to collect microphone and LED signals. Satisfactory synchronization, observed over all frequency ranges tested, provided confidence in the acquisition process.

2.2. Signal processing and experimental uncertainty

The details of the signal processing for calibrating the photo-electron counts to density, measuring time-averaged density, density fluctuations spectra via cross-correlating the time signature obtained by the two PMT can be found in PS and Panda *et al.* (2004). The primary source of uncertainty in the measurement of the time-averaged density is from the electronic shot noise, which is minimized via averaging over long time duration. Secondary sources from neglecting the change of Rayleigh-scattering cross-section and occasional passage of particles introduced an uncertainty of $\pm 2\%$ to the time-averaged $\bar{\rho}$ measurement. The standard deviation of density fluctuations ρ'_{rms} was measured by integrating the density fluctuation spectrum. This process mostly avoided contributions from the electronic shot noise; however, very low levels of density fluctuation found inside the potential core of the jets could not be measured. Another source of error in the spectral data was from the passage of occasional particles or traces of condensation droplets (for unheated plumes) through the probe volume. The passage of such particles increases the correlated part of the signal in both PMT counts. This leads to a bias towards higher value in the density spectrum

calculation as well as the root-mean-square calculations. As the probe volume was moved from close to the nozzle exit to 15 diameters downstream, the number of particles increased progressively from a few per second to the order of 1000 per second. Signatures of large particles are identifiable as large pulses in the time series of photo-electron counts and are discarded. However, the signature of smaller particles passing through the vicinity of the beam waist could not be discarded. It is estimated that, on an absolute level, a bias of $\rho_{rms} \sim 0.014 \text{ kg m}^{-3}$ was present in the r.m.s. data. The non-dimensionalization by $|(\rho_j - \rho_a)|$ placed this bias at different levels, seen in the figures presented later in this paper. The situation is worst for the unheated jet where $|(\rho_j - \rho_a)|$ is small. The bias error increased as a larger number of particles was entrained into the jet. No data were taken beyond a downstream distance of $15D$.

Calculations of the flow-sound correlation coefficient required ρ'_{rms} estimates which required subtraction of the shot noise contribution. The procedure followed is the same as discussed in PSE. Briefly, the cross-correlation was calculated via inverse Fourier transform F^{-1} of the cross-spectrum:

$$\langle \rho'; p' \rangle = \frac{F^{-1}(F_N(1)F_{p'}^*(1))}{k\Delta t^2} \quad 1 = 0, \pm 1, \pm 2, \dots, \pm \frac{1}{2}n-1. \quad (3)$$

Where, F represents Fourier transform, superscript $*$ represents a complex conjugate, Δt is the sampling interval and n is the number of data points used for the transform. Since electronic shot noise is present only in the density data, the cross-correlation process rejects its contribution. While un-normalized $\langle \rho'; p' \rangle$ is accurate, the primary source of uncertainty creeps in via estimates of ρ'_{rms} that had to be measured from individual PMT. In general, an uncertainty of $\pm 10\%$ is expected in the normalized correlation coefficients $\langle \rho'; p' \rangle / (\rho'_{rms} p'_{rms})$.

3. Results and discussion

The following discussion is based on two sets of results. The larger first set is from jets with different temperature ratios but fixed acoustic Mach number $M_a = 0.9$. The smaller second set is from jets of different acoustic Mach number but at constant temperature ratio $T_r = 2.27$. The aerodynamic Mach numbers for all jets were subsonic ($M_j < 1.0$); hence, shock waves were absent.

3.1. Time-averaged and r.m.s. data

$M_a = 0.9$ plume survey

Figure 3 presents density survey from one of the heated plumes. The overall shapes and progressive changes are typical of all plumes: heated or unheated. The unheated jet has a higher core density than the ambient ($\rho_j > \rho_a$) owing to isentropic cooling from plenum temperature. The heated jet, on the other hand, has a lower density than the ambient ($\rho_j < \rho_a$). The experimental data are non-dimensionalized by the difference between the jet centreline and the ambient density, $(\rho_j - \rho_a)$. The time-averaged data were non-dimensionalized as $(\bar{\rho} - \rho_a) / (\rho_j - \rho_a)$. The parameter is unity at the core and drops to zero as the ambient condition is reached, regardless of whether the core density is higher or lower than the ambient. For a similar reason, the fluctuating density data were normalized by the absolute value of the density difference: $\rho_{rms} / |(\rho_j - \rho_a)|$. The radial profiles show progressive growth of the lip shear layer and the expected spreading of the plumes. Detailed radial surveys, from other operating conditions, show similar trends to those in this figure.

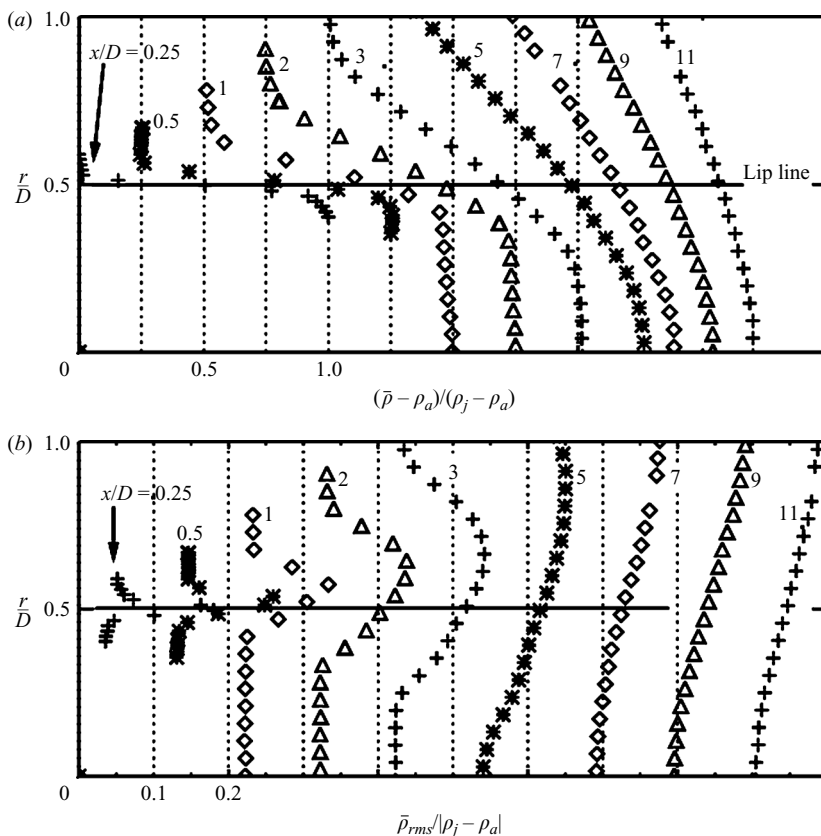


FIGURE 3. Radial profiles of (a) mean and (b) r.m.s. density variations in $T_r = 2.7$, $M_a = 0.9$ jet from indicated axial stations.

A closer look into the r.m.s. data along the lip line shows a difference between the unheated and heated jets. The peak density fluctuations, at the first measurement station, appear close to the lip line. This peak position, however, moves inward towards the centreline in the unheated jet, while in the heated jet the peak location moves radially outward. To further examine this difference, time-averaged and r.m.s. density profiles from a single axial station are plotted in figure 4. The figure shows that while profiles from all heated conditions are nearly similar, the profile of the unheated jet is narrower, perhaps indicative of slower spreading. Now, radial spreading seen via density measurement is found to be different from that seen via axial velocity measurement. Figure 5 presents a comparison of the present density data with velocity data measured in the same facility by Bridges & Wernet (2003). The velocity profiles of figure 5(a) are almost self-similar: they collapse onto a single line when plotted without shift. The density shear layer, on the other hand, lies inside the velocity shear layer in the unheated jet, but moves outside whenever heating is introduced. The velocity and density data are from two different experiments and therefore, a small difference in the radial positions of the probe volume is expected. The differences seen in figure 5, however, are larger than the positioning error. The Crocco–Busemann equation (White 1973) also predicts similar differences between velocity and density shear layers for heated and unheated conditions. Assuming unit Prandtl number the Crocco–Busemann equation describes total enthalpy variation as a linear function of

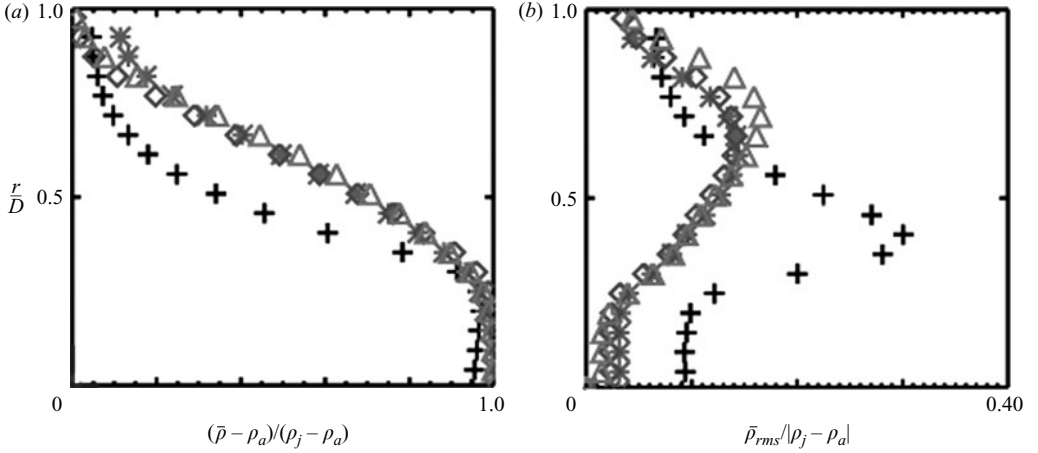


FIGURE 4. Radial profiles of (a) mean and (b) r.m.s. density variation at fixed axial position of $x/D=3$, and fixed $M_a=0.9$, but for different plume temperatures. +, $T_r=0.84$; *, 1.43; ◇, 1.82; Δ, 2.7.

velocity. With an additional assumption of constant ratio of specific heats γ , it can be written in terms of M_a and T_r as:

$$\frac{\bar{\rho} - \rho_a}{\rho_j - \rho_a} = \frac{T_r}{1 - T_r} \left\{ \left[1 - \frac{\gamma - 1}{2} M_a^2 \left(\frac{\bar{U}}{U_j} \right)^2 + \left(\frac{\gamma - 1}{2} M_a^2 - 1 + T_r \right) \frac{\bar{U}}{U_j} \right]^{-1} - 1 \right\}. \quad (4)$$

The solid line in figure 5(a) shows the predicted density variation from the velocity profile using (4). In spite of the small differences in the probe location, the predicted density profile also shows the same difference between the unheated and heated jets as seen in the Rayleigh data.

The pitfall in normalization by $(\rho_j - \rho_a)$ is that in a temperature-balanced jet the terms become zero. The temperature-balanced jets ($T_j = T_a$) are produced by slight heating of the primary jet to counterbalance cooling from the expansion process. The density fluctuations in such a jet were also measured in the present test. The radial time-averaged density profiles measured in such jets (not shown) show an interesting dip in the middle of the shear layer. Because of the viscous heating, the static temperature at this location becomes higher than that of the plume, resulting in a lowering of density. The Crocco–Busemann equation was found to predict this dip correctly.

The radial profiles of the root-mean-square density fluctuations are found to be somewhat different from those of the axial velocity. This may be of interest for turbulence and noise source modelling. Figure 5(b) shows that the radial location for the peak density fluctuations moves further away from that of the axial velocity as the plume temperature is increased. Therefore, the absolute magnitude of the density–velocity correlation is expected to change with heating. Intuitively, the trend makes sense: in the unheated jet, core density is higher than the ambient; therefore the growth of the shear layer is accompanied by higher-density fluctuations in the core side. An opposite situation arises in heated jets where the ambient density is higher than the core.

Leaving aside the difference between the heated and unheated conditions, when only the heated jets are considered, figure 4 shows that there exist small differences in the spreading. This was also confirmed from the measured centreline data (not

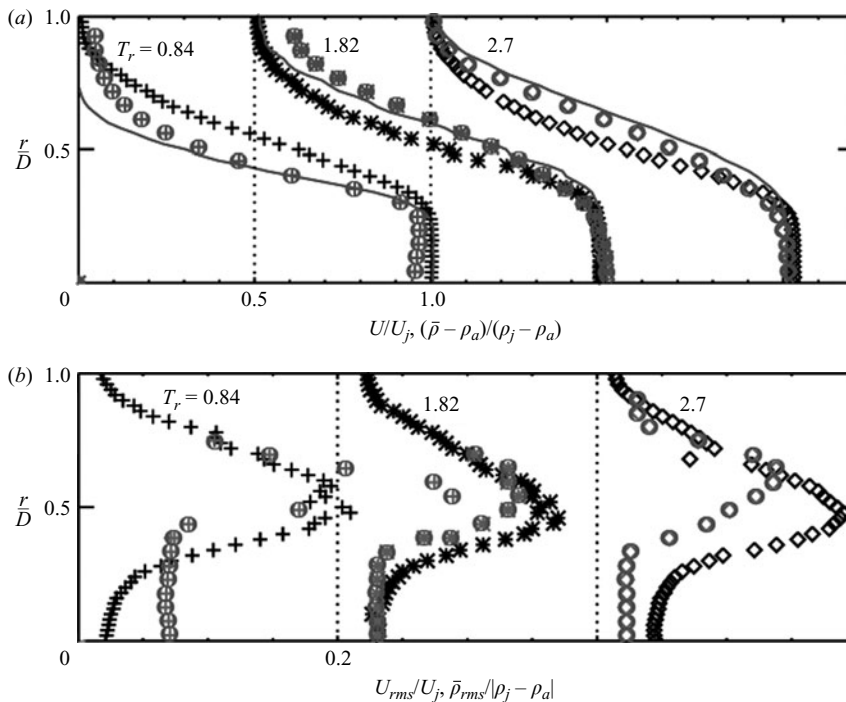


FIGURE 5. Radial profiles of (a) mean axial velocity and density (circled symbols) variations and (b) r.m.s. velocity and density variations from fixed axial position of $x/D=3$, and fixed $M_a=0.9$, but for different plume temperatures. The axial velocity data were from PIV measurements of Bridges & Wernet (2003). The axial velocity data in (a) shows the predicted density profile from velocity data using the Crocco–Busemann relation. The profiles are shifted by the amounts shown by chain lines.

presented). To identify the changes in spreading owing to heating, we must survey jets with constant aerodynamic Mach number M_j , a parameter that quantifies the compressibility effect. The present experiment was conducted in constant acoustic Mach number M_a where M_j is shown to decrease continually with heating. Lau (1981) and Lepicovsky *et al.* (1988) have shown that the spreading rate increases with heating. The current trend is perhaps due to viewing the jet through density, and a cancellation between a decrease in the spreading rate due to the lowering of M_j , and an increase in the spreading rate due to increasing plume temperature.

Figure 6 presents data from the second set of operating conditions where jet velocity was varied, keeping temperature constant. For these plumes, increase in the jet velocity is accompanied by a similar increase in the aerodynamic Mach number M_j and the associated lowering of the shear-layer growth rate. This manifests in a longer potential core length with increasing M_a . The rate of growth of the r.m.s. density fluctuation for $x/D > 5$ is markedly different in the highest $M_a = 1.48$ jet. This might be a manifestation of the compressibility effect and should be studied in association with simultaneous velocity fluctuations measurements. Such studies are planned for the future.

3.2. Density fluctuation spectra

Density fluctuation spectra measured from the heated $T_r = 2.7$ jet are shown in figure 7. The power spectral values are normalized by $(\rho_j - \rho_a)^2$, and the Strouhal

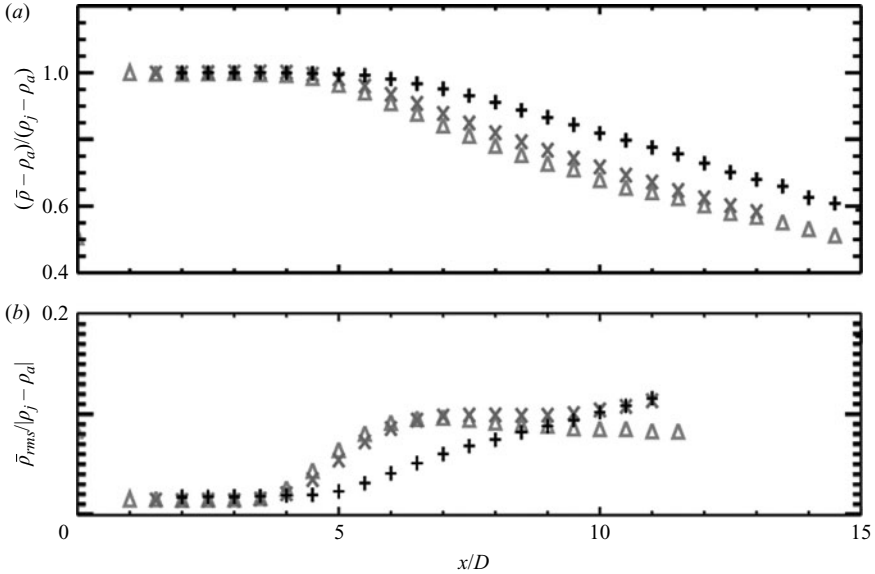


FIGURE 6. Centreline variation of (a) time averaged density and (b) r.m.s. density fluctuations in jets with different indicated acoustic Mach numbers but fixed static temperature ratio, $T_r = 2.27$. Δ , $M_a = 0.6$; \times , 0.9; +, 1.48.

frequency band ΔSt . The digital power spectral calculations provided mean-square fluctuations within a frequency band Δf for different centre frequencies f . The centre frequencies were converted to Strouhal numbers and the band to $\Delta St = \Delta f D / U_j$. The potential core region of the jet has little fluctuation; the spectrum at $x/D = 3$ in figure 7(a) is mostly indicative of the electronic noise floor. Along the centreline, the spectral energy starts to grow as the end of the potential core is approached ($x/D \sim 5$), and remains high for the rest of the measurement locations. The spectral energy is expected to decay farther downstream of the last measurement station. The peripheral shear layer (figure 7b) was highly turbulent even at the first measurement station: $x/D = 0.25$. In fact, the spectral energy level is higher at the first measurement station than at all other downstream locations; the high-frequency part relaxed to lower levels within a short distance. The r.m.s. density fluctuation data, presented earlier, show that the peak fluctuation region moves radially away from the lip line. This is an additional reason for the lowering of spectral energy seen in figure 7(b). A comparison with earlier measurements (PS) in unheated jets shows significant differences in the density spectra measured along the shear layer. The data of PS showed a progressive increase in the energy level with downstream distance. The spectral shape was also different: a hump at $St \sim 4$ was present in the spectrum close to the nozzle exit. The hump progressively moved to lower Strouhal frequencies with downstream distance. The behaviour was typical of a quasi-laminar shear layer going through transition to full turbulence. The data of figure 7(b), however, indicate a fully turbulent shear layer right at the nozzle exit.

Spectra from plumes of different temperature ratios but at a fixed $M_a = 0.9$ are compared in figure 8. Notably, the spectra from heated conditions show little difference within measurement uncertainty. The unheated jet data in figure 8(b) stands out to show higher energy level which is the result of the trace condensation produced in

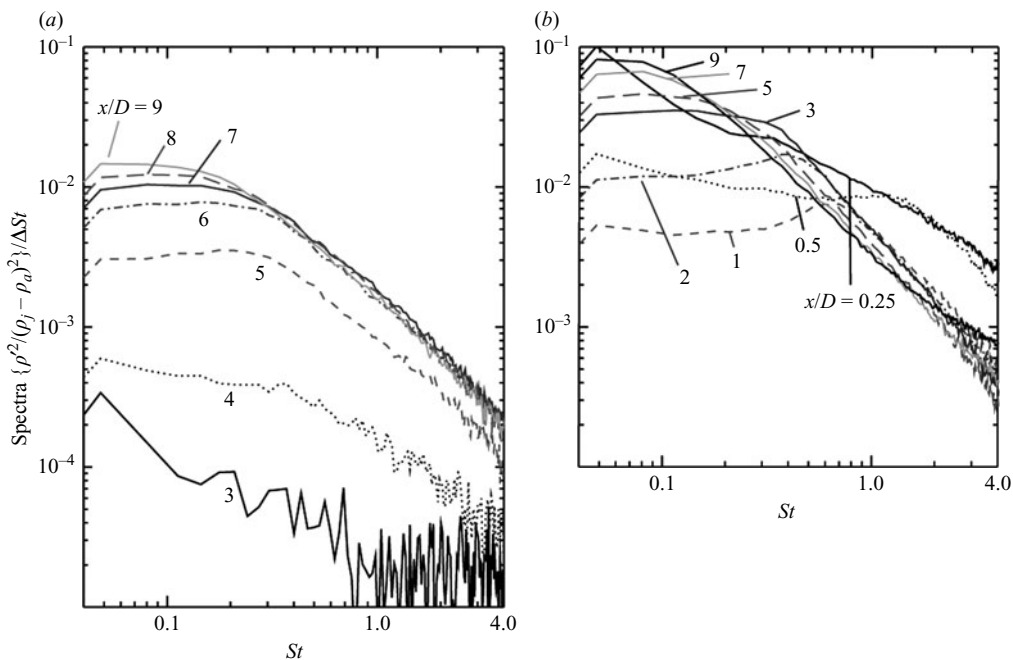


FIGURE 7. Density fluctuations spectra from indicated axial stations along (a) centreline and (b) lip line of $M_a = 0.9$ and $T_r = 2.7$ jet.

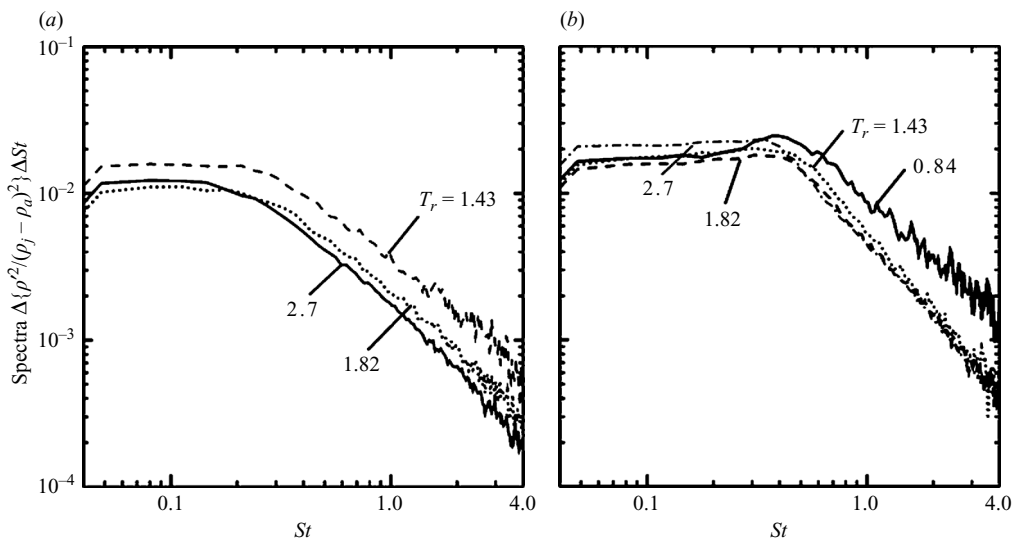


FIGURE 8. Density fluctuation spectra from jets of different temperature ratios but fixed $M_a = 0.9$. Position of probe volume was kept fixed at (a) centreline and $x/D = 8$ and (b) $r/D = 0.54$ and $x/D = 3$.

the cold plume discussed earlier. Nevertheless, it is reasonable to conclude that the density fluctuation spectra uniformly scale as $(\rho_j - \rho_a)^2$.

Density fluctuation spectra from plumes of fixed static temperature but different jet velocities are compared in figure 9. Except for the small differences in the

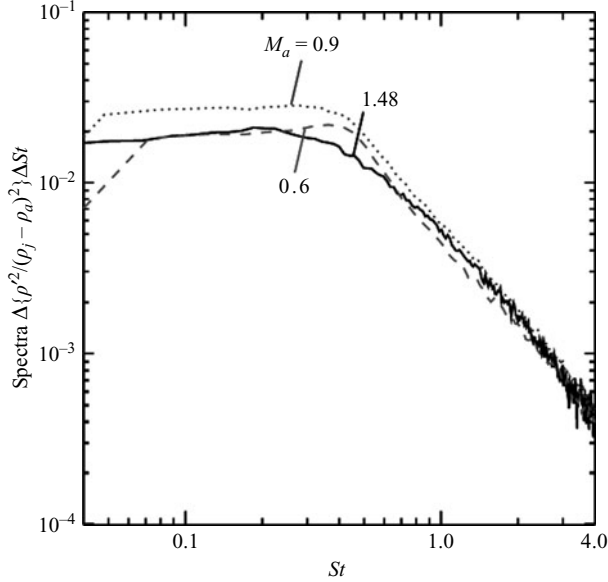


FIGURE 9. Density fluctuation spectra from jets of different indicated Mach numbers but a fixed temperature ratio of $T_r = 2.27$. Probe volume was kept fixed at $r/D = 0.54$ and $x/D = 3$.

low-frequency end, spectra are strikingly similar over the wide range of plume velocities. PS found similar results over a wider Mach-number range in unheated jets via plume survey. Figures 8 and 9 show that the single-point statistics of turbulence fluctuations remain more or less similar over the wide velocity and temperature ranges considered in these experiments. The magnitude of turbulent density fluctuations is proportional to the difference of the air density between the jet core and the ambient. This is in contrast to the large change in the far-field noise spectra measured in these jets. The single-point turbulent statistics are primarily indicative of the mixing between the ambient and the jet fluid, and perhaps are ineffective in demonstrating the dynamic process responsible for the noise generation.

Initial shear layer

The effect of heating on the fluctuations present in the initial shear layer close to the nozzle exit is investigated in figures 10 and 11. The non-dimensionalized time-averaged density profiles of figure 10, at all plume temperatures, are nearly similar. The peak r.m.s. fluctuations in the lip shear layer increase with increased plume temperature. The density fluctuation spectra in figure 11 provide additional support. The spectra show that the unheated jet has lower energy levels at the lower frequencies than any of the heated jets. The spectra from the unheated jet shows a hump around $St = 4$, similar to the quasi-laminar shear layer of PS. Noticeably, the low-frequency part of the spectrum becomes more energetic with increased plume temperature. It has been discussed earlier that increasing plume temperature at constant velocity reduces Reynolds number. Table 1 shows Reynolds-number reduction from 1.4×10^6 in the unheated condition to 0.2×10^6 in $T_r = 2.7$ jet. Therefore, before the test, it was expected that laminarization of the initial shear layer would be found with increased heating. Figure 11 shows an opposite trend: an increase of the fluctuation level with heating. It is conjectured that one or more of the following possibilities give rise to the increased turbulence. First, the increased strength of the Görtler vortices generated

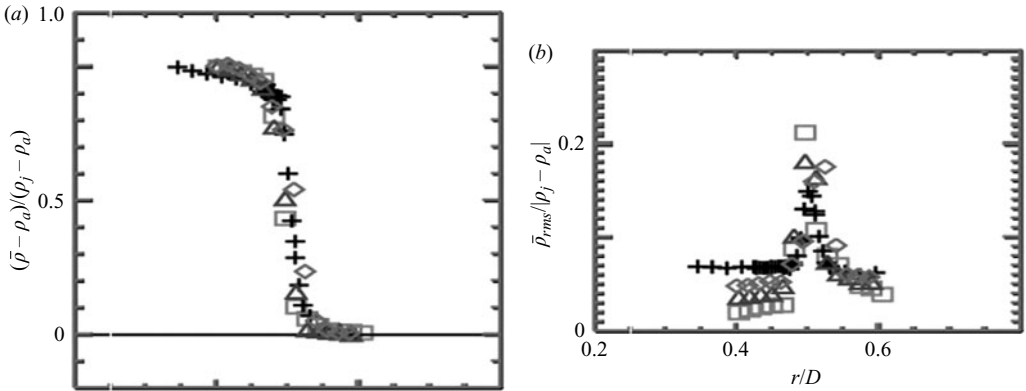


FIGURE 10. Radial profiles of (a) mean and (b) r.m.s. density variation from close to the nozzle exit, $x/D = 0.25$, from jets of different temperature ratios but fixed $M_a = 0.9$. +, $T_r = 0.84$; \diamond , 1.43; Δ , 1.82; \square , 2.7.

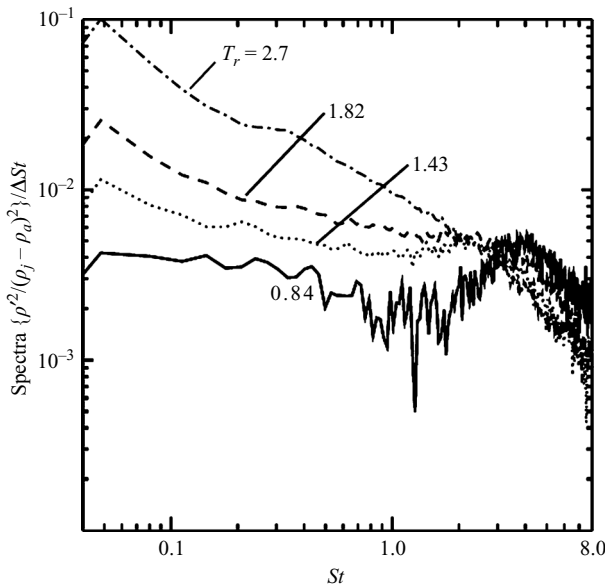


FIGURE 11. Density fluctuations spectra from locations of maximum ρ_{rms} in lip shear layer close to the nozzle exit, $x/D = 0.25$. Data from jets of different temperature ratios but fixed $M_a = 0.9$.

at the concave part of the nozzle contraction. The strength of such vortices may increase with heating and the associated lowering of the local Reynolds number. Secondly, an onset of the instability of the low-density jet column (Monkewitz *et al.* 1990; Russ & Strykowski 1993). Thirdly, an appearance of a locally separated region of flow upstream of the contraction section. It is known from various low-Reynolds-number-wind tunnel performances that the wall boundary layer at the beginning of a contraction section experiences adverse pressure gradient owing to curvature of streamlines (Morel 1975). Since the flow velocity is very low, small local separation is not uncommon. Viswanathan & Clark (2004) computed flow field inside contraction

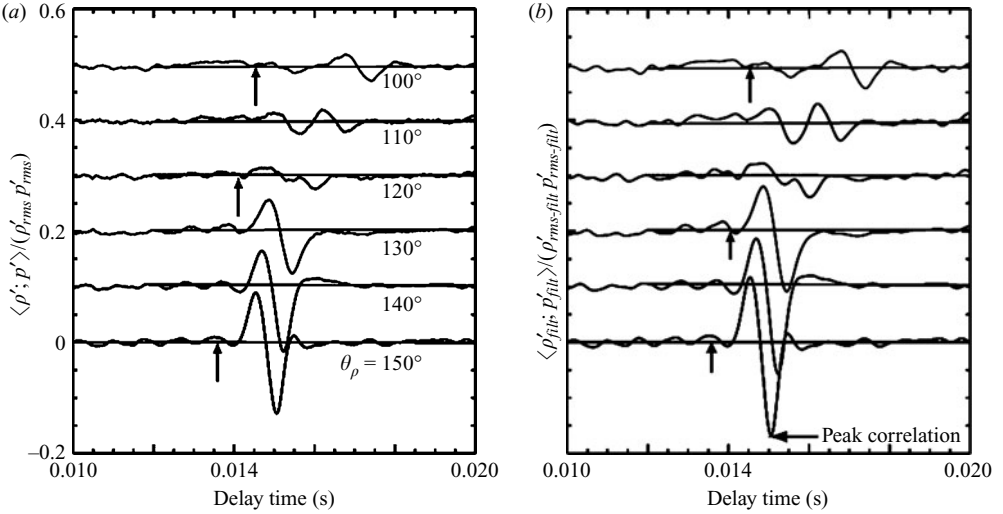


FIGURE 12. Normalized correlations between turbulent density fluctuations and far-field sound pressure fluctuations measured from a fixed laser probe location with microphones placed at indicated polar angles (θ_p). The laser probe is kept fixed at $x/D=9$, $r/D=0$ in $M_a=0.9$, $T_r=2.7$ jet; microphones were located on a $100D$ arc. (a) Correlations from all frequencies (b) that from $0 \leq St \leq 0.5$ filtered range. Vertical arrows show free-space propagation time of sound from laser probe to microphone.

sections of different geometries and found significant flow separation for many of these sections.

3.3. Flow–sound correlation

Noise sources in the heated plumes were identified via correlating density fluctuations measured by the laser probe, with far-field sound pressure fluctuations, measured by microphones. Figure 12 presents correlation data from the strongest sound-generating part of the plume. This figure has many similarities with data presented in PSE and corroborates the observations presented therein. Similar to the earlier data, magnitudes of correlations are found to decrease with the polar angle. Also correlations appear at longer time delays than the time required for sound waves to travel from the laser probe to the microphone without any flow–acoustic interaction. Sound waves either take a longer route or encounter a slower speed over a part of the propagation distance. There is a difference in the shapes of the correlation curve between the prior unheated jets and the present heated jets. Data from the heated jets shown in figure 12 universally show weak positive peaks followed by strong negative peaks, whereas data from unheated jets (PSE) shows a weak negative peak followed by a stronger positive peak. Recall that unheated jets plumes have higher densities than the ambient; whereas heating causes a reversal. That the correlation curve also switches shape based on whether the plume is lighter or denser than the ambient is perhaps indicative of the same noise-generation mechanism based on the momentum exchange between the peripheral and the core part of the jet. Such an exchange would have allowed for the laser probe to sense higher density than average in unheated jets and lower density in heated ones for the same part of the radiated sound wave.

Frequency analysis of the correlation data showed that fluctuations from the low-frequency range $0 < St < 0.5$ primarily contributed towards the correlation; the rest fell below the experimental noise floor. The entire broadband fluctuations were

used to calculate correlations in figure 12(a). For figure 12(b), both microphone and density time traces were digitally filtered (frequency domain, Butterworth-like) between $St = 0.0$ to 0.5 before cross-correlating. Figure 12(b) shows an improvement in the absolute magnitude of correlation, leaving the shape and other details intact. Unfiltered correlations are used in the rest of the paper.

Figure 13 presents the effect of increasing plume temperature, keeping velocity constant, on the peak correlation coefficient. Note that the absolute magnitude $|\langle \rho'; p' \rangle|_{max}$ was used. The negative peak in the correlations from the heated jets and the positive peak for the unheated jet were used in this figure. In figure 13(a–d), the laser probe was moved from point to point nominally along the lip-line. For each probe location, correlations from all six microphones were calculated. For figure 13(e–i), the laser probe was moved nominally along the centreline. Figure 13 demonstrates a direct relationship between the plume temperature and correlation coefficients: an increase in one is reflected similarly in the other. The increase is more prominent in the peripheral shear layer which hardly radiates in the unheated subsonic jet, yet becomes increasingly efficient as T_r is increased. If the correlation coefficient is broadly interpreted as the efficiency factor of a unit mass of air at the probe location to radiate to the microphone, then an improvement of this efficiency with increased plume temperature is apparent from this figure. (Panda *et al.* (2004) presented correlation data in the form of coherence spectra. Unlike the time domain correlation values presented in figure 13, coherence spectra are heavily affected by electronic shot noise. This was particularly true for the $T_r \sim 1.0$ jet where the plume and the ambient had nearly the same time-averaged density. These led to a very small level of fluctuating density and ultimately nearly zero coherence. Some of the conclusions drawn in that paper based on the coherence spectra are now corrected.)

Finally, figure 14 presents the effect of increasing plume velocity, keeping temperature constant, on the correlation coefficients. Similar to the earlier results from the unheated jets (PS), increasing jet velocity is found to improve the correlation coefficients significantly. The differences are more significant along the peripheral shear layer where strong correlations found in the $M_a = 1.48$ jet are mostly absent in the $M_a = 0.6$ jet. As the jet speed approaches and exceeds the ambient sound speed, the fluctuations present in the peripheral shear layer become more and more efficient radiators. Additionally, frequency analysis of the correlation data shows that the frequency range over which correlations can be measured becomes wider with increasing jet velocity. While Strouhal frequencies in the range 0–0.5 correlate in a $M_a = 0.9$ jet, the range extends to 0–1.0 in a $M_a = 1.48$ jet.

4. Effect of heating on far-field noise spectra

Although the subject has been discussed by many workers, the present section looks into the issue from the perspective of a major observation made from the preceding correlation study: the efficiency of low-frequency noise production per unit mass of the jet flow increases with heating. In this section, the effect of heating on far-field noise spectra is discussed using data from prior workers (Tanna *et al.* 1976). The microphone signals obtained from the present test were contaminated by unavoidable reflections from large lenses and other optics placed in the vicinity of the jet flow. The signals were sufficiently clean for the flow–sound correlation study, yet unsuitable for studying finer details of the far-field noise spectra.

The overall level in the far-field noise spectrum is a function of many parameters; the most influential of all is the jet efflux velocity. In order to isolate the effect

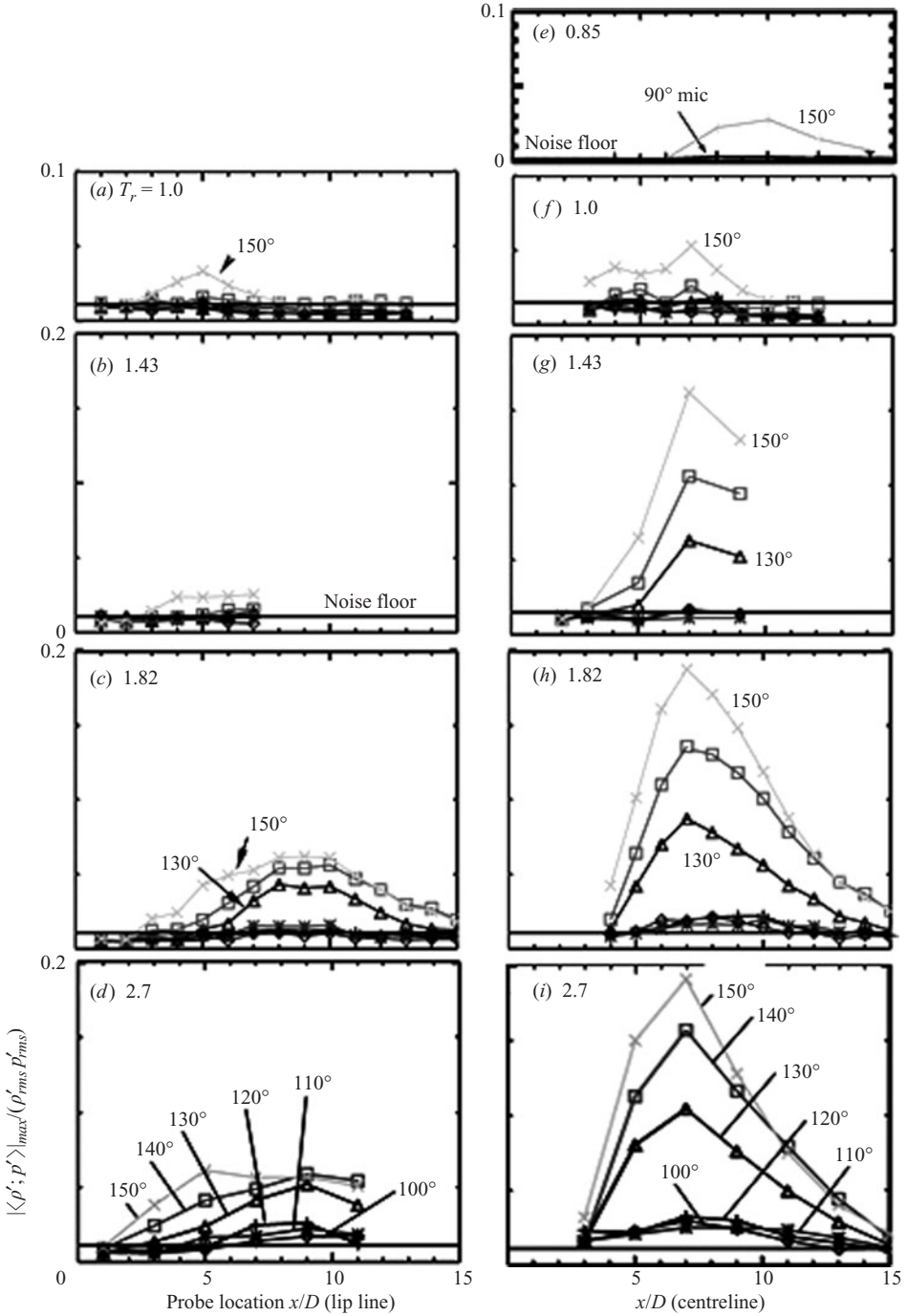


FIGURE 13. Temperature dependence of the peak correlation coefficients for fixed velocity plumes: $M_a = 0.9$. The plume temperature ratios are as indicated; different curves in each plot correspond to different microphone polar angles as indicated. The laser probe was moved nominally along the lip line for (a)–(d) and nominally along the centreline for (e)–(i). All microphones were on a $100D$ arc. The unheated jet data in (e) is from Panda *et al.* (2005).

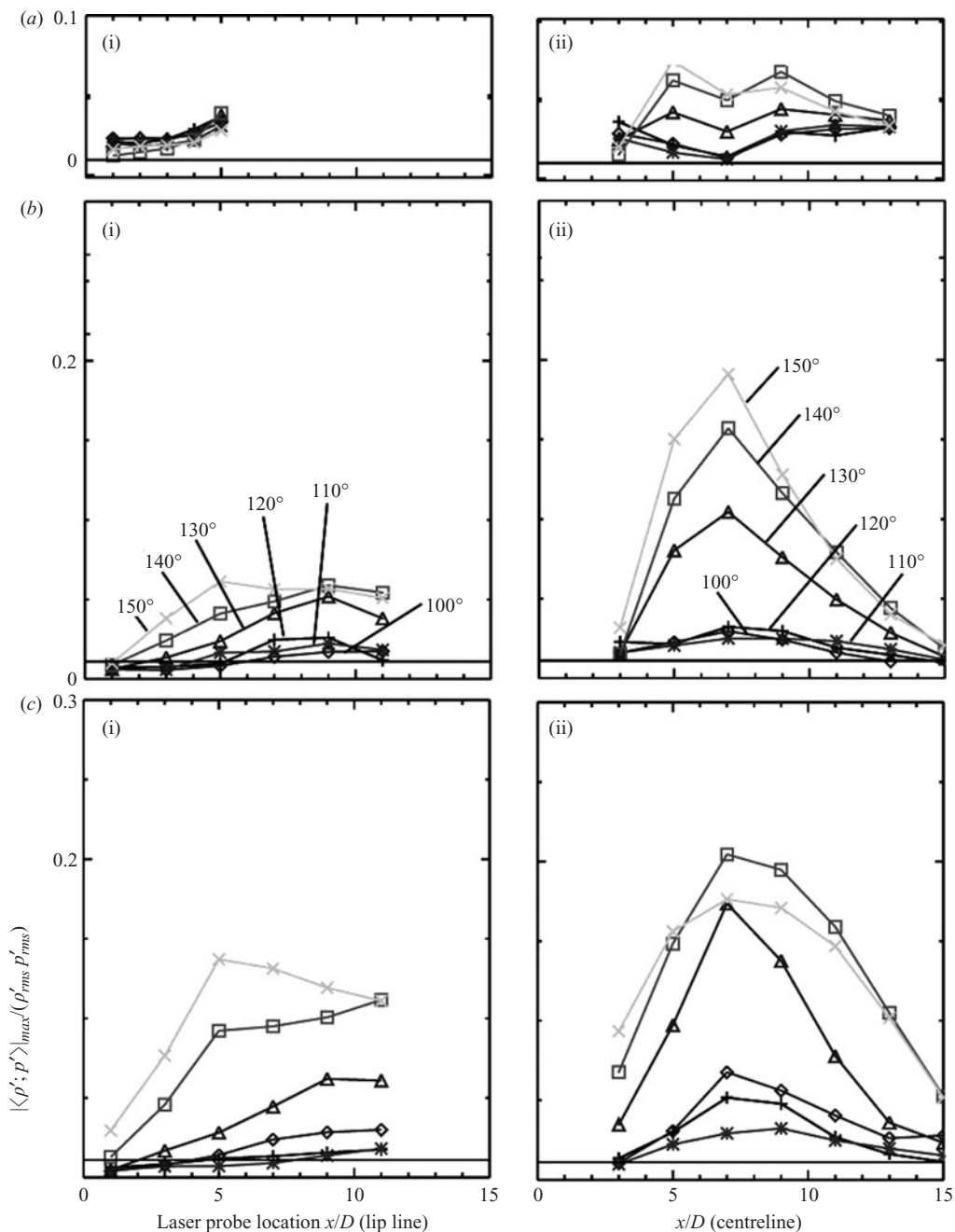


FIGURE 14. Mach number (acoustic) and polar angle dependence of peak correlation coefficients. The laser probe was moved at different axial positions nominally along (i) lip line $r/D=0.5$ and (ii) centreline $r/D=0$. (a) $M_a=0.6$, $T_r=2.27$; (b) 0.9 , 2.7 ; (c) 1.48 , 2.27 . Different curves in each plot are for different microphone polar angles as indicated. The symbols are consistent throughout the plot.

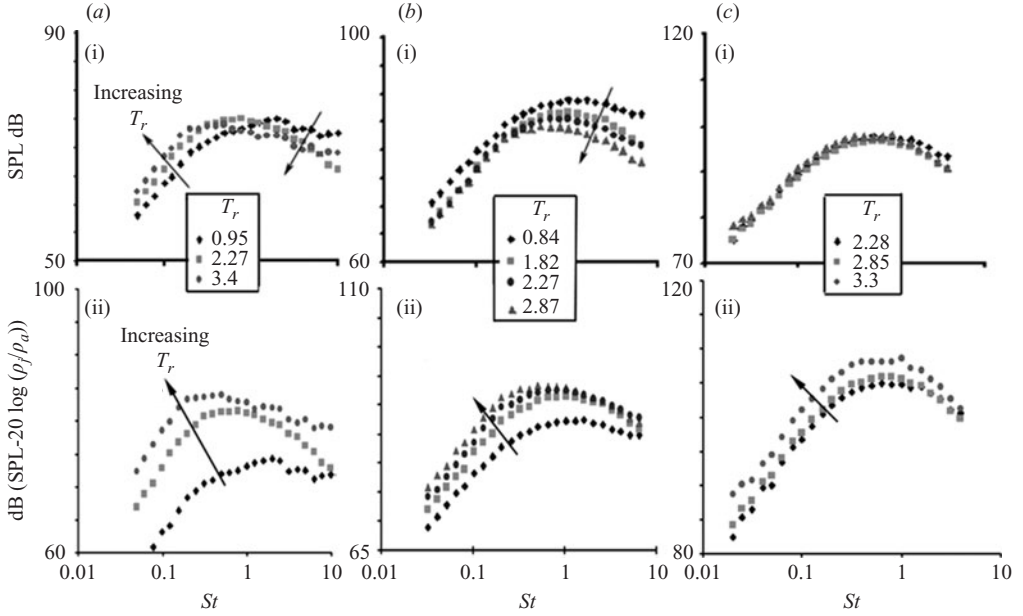


FIGURE 15. As-measured and density normalized far-field noise spectra at 90° to the jet axis from jets at fixed velocity but different temperature ratios. Measured data from Tanna *et al.* (1976). (a) $M_a = 0.6$, (b) 0.9 , (c) 1.48 .

of heating, we must change the plume temperature/density while keeping all other parameters constant. Past studies on the influence of heating were performed in fixed-diameter round jets keeping the efflux velocity (and thereby the acoustic Mach number $M_a = U_j/a_0$) constant, while varying the temperature ratio ($T_r = T_j/T_{amb}$). Such studies have shown intriguing, difficult to interpret, effects that depend on the chosen M_a . The problem arises from the accompanying reduction in the air density ρ_j , which reduces the mass flow rate (proportional to $\rho_j U_j D^2$) and the net thrust (proportional to $\rho_j U_j^2 D^2$) produced by the jet. The changes are significant: a jet with a fixed diameter D and fixed velocity U_j at a $T_r = 2.7$ has only 37% of the mass flow rate (thrust) compared to the unheated counterpart. To compensate for the mass flow rate reduction (thrust loss), we must use larger diameter nozzles with increasing plume temperature. However, almost all existing studies considered the effect of heating using a fixed-diameter nozzle. Therefore, to account for the change in the mass flux, a density-based scaling law must be used. Unfortunately, many of the existing scaling laws (Goldstein 1976; Lilley 1991) use only the ambient density, and therefore, are unsuitable for the problem. Since, for a fixed U_j and D , mass flow rate is proportional to the jet density, in the following an attempt is made to scale the far-field spectra using ρ_j . With the ambient density ρ_a as a suitable non-dimensionalizing parameter, a corrected sound pressure level SPL is defined as:

$$(SPL)_{corrected} = 20 \log \left(\frac{p'_{rms} \rho_a}{P_{ref} \rho_j} \right).$$

Since the data available in the literature defines

$$SPL = 20 \log \left(\frac{p'_{rms}}{P_{ref}} \right) \text{ hence } (SPL)_{corrected} = SPL - 20 \log \left(\frac{\rho_j}{\rho_a} \right), \quad (5)$$

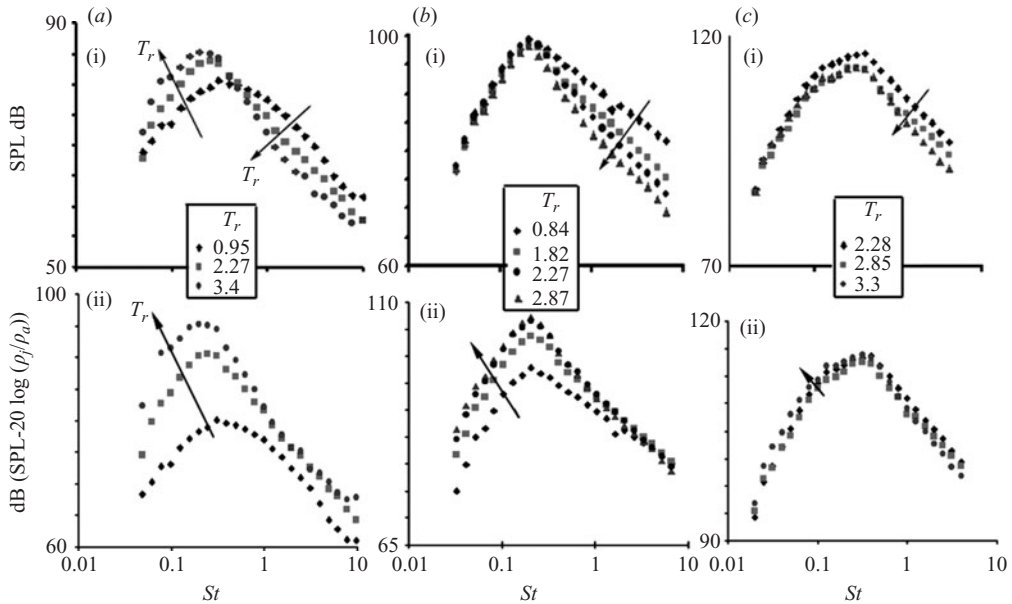


FIGURE 16. Same as figure 15, except for the microphone polar angle of 150° .

where, $P_{ref} = 2 \times 10^{-5} \text{ N m}^{-2}$. A comparison between far-field noise spectra, plotted with and without the correction, at two different microphone polar angles, is shown in figures 15 and 16. All uncorrected data presented in these figures are from Tanna *et al.* (1976) who used a 50.8 mm diameter convergent round nozzle to produce the plumes. Microphones were kept on a $72D$ arc. The uncorrected data show the complex temperature dependencies described by Fisher *et al.* (1973), Hoch *et al.* (1973) and Tanna (1977). The acoustic spectra show an increase in low-frequency noise and a decrease in the high-frequency noise with heating. The cross-over frequency and the extent of change are functions of sensor polar angles and M_a . The corrected data significantly clarify the ever-increasing low-frequency noise with increasing temperature. The increase is seen at all polar angles, and Mach numbers M_a . The low-frequency part of the spectrum increases more rapidly with T_r , than the high-frequency part. The corrected spectra further support the observation that heating increases efficiency of noise production per unit mass flow rate/thrust produced by the jet. Furthermore, like the correlation data, the increase in noise is most prominent in the low-frequency part of the spectrum.

5. Summary and conclusion

A molecular Rayleigh-scattering-based density-measurement technique was used in a small hot jet acoustic rig to investigate turbulence properties and noise sources of hot high-speed jets. Rayleigh scattering was used in the past to diagnose noise sources in unheated jets (PS); this study was the counterpart in heated jets. A large amount of flow and acoustic data were obtained over different acoustic Mach numbers and temperature ratios. Additionally, unsteady density fluctuations ρ' in the jet and sound pressure fluctuations p' at far-field microphone locations were measured simultaneously. A cross-correlation $\langle \rho'; p' \rangle / (\rho'_{rms} p'_{rms})$ between the two fluctuations

provided information about the low-frequency noise sources. All of these efforts resulted in many new observations which are summarized below.

The correlation coefficients were found to improve progressively with increased plume temperature in jets where plume velocities were kept fixed at $M_a = 0.9$. The increase was most impressive when the laser probe was placed at points along the lip shear layer. The correlation coefficients from these regions were in the experimental noise floor in unheated plumes, yet showed significant improvements with heating. The normalized correlation coefficients provide a measure of noise radiation efficiency at the probe location. An increase in the correlation coefficient is indicative of higher radiation efficiency. Therefore, heated jets with constant mass flow rate and efflux velocity are expected to radiate higher noise levels with heating.

An examination of the existing far-field noise data from heated jets provided further support for this observation. Traditionally, to determine the effect of heating, a comparison is made between noise spectra measured from plumes with constant efflux velocity, produced from a fixed diameter nozzle, while varying the static temperature. Increasing plume temperature reduces density, and thereby, the mass flow rate and the thrust produced by the jet are also lowered. It is, therefore, proposed to normalize far-field noise spectra by plume density. Such corrected spectra provide comparison in far-field noise generated from equal acoustic Mach number M_a and mass flow rate (thrust level) jets. Noise spectra measured by Tanna *et al.* (1976) were re-plotted with this correction, and found to demonstrate a consistent increase in noise level at all frequencies and polar angles with increasing plume temperature. The increase is more pronounced at lower jet velocities and at the low-frequency end of the spectrum. This is consistent with the observations made from the correlation study.

To identify the effect of increasing velocity, correlation coefficients were measured in three plumes of $M_a = 0.6, 0.9$ and 1.48 , and at nominal $T_r = 2.27$. Similar to the prior results in unheated jet (PS; PSE), correlation values measured in the heated jets are also found to increase progressively with increasing velocity. Once again, the increase was remarkable when the laser probe was placed at points along the lip line. The increase in the correlation coefficient is once again consistent with trends in far-field noise spectra.

Detailed surveys of the density field (time-averaged and fluctuation spectra) were conducted in all plumes. The time-averaged density measurements at fixed M_a but different T_r showed differences in the peripheral density shear layers between the unheated and heated conditions. Comparisons with earlier axial velocity data from PIV survey of Bridges & Wernet (2003) show that in the unheated jet, the density shear layer hugs the inside edge of the velocity shear layer, whereas in the heated jet, the density shear layer lies on the outside edge. Peak density fluctuation is found to lie at larger radii than that of the axial velocity fluctuations.

The density fluctuation spectra measured at the closest axial station, $x/D = 0.25$, and at the middle of the lip shear layer showed an unexpected increase in the low-frequency content with increased heating. The downstream development of the lip shear layer was typical of a fully turbulent jet, unlike the transitional behaviour seen in unheated jets of PS. Further downstream from the nozzle exit, the density fluctuation spectra normalized by $(\rho_j - \rho_a)^2$ were mostly similar for all temperature-ratio and Mach-number conditions. This demonstrated a near universality of single-point statistics of the turbulence field.

The author acknowledges support from the Ultra Efficient Engine Technology program of NASA in performing this experiment. Help in instrumentation and

data acquisition from Dr Richard G. Seasholtz (retired), Ms Amy F. Mielke of NASA Glenn Research Center and Ms Kristie A. Elam of Jacobs Sverdrup are also acknowledged.

REFERENCES

- BOGEY, C. & BAILLY, C. 2005 Investigation of sound sources in subsonic jets using causality methods on LES data. *AIAA Paper* 2005-2885.
- BRIDGES, J. & BROWN, C. A. 2005 Validation of the small hot jet acoustic rig for aeroacoustics research. *AIAA Paper* 2005-2846.
- BRIDGES, J. & WERNET, M. P. 2003 Measurements of the aero-acoustic sound source in hot jets. *AIAA Paper* 2003-3130.
- DOTY, M. J. & McLAUGHLIN, D. K. 2003 Acoustic and mean flow measurements of high-speed, helium air mixture jets. *Intl J. Aeroacoust.* **2**, 293–333.
- FISHER, M. J., LUSH, P. A. & HARPER-BOURNE, M. 1973 Jet noise. *J. Sound Vib.* **28**, 563–585.
- FREUND, J. B. 2002 Turbulent jet noise: shear noise, self noise and other contributions. *AIAA Paper* 2002-2423.
- GOLDSTEIN, M. E. 1976 *Aeroacoustics*. McGraw-Hill.
- HOCH, R. G., DUPONCHEL, J. P., COCKING, B. J. & BRYCE, W. D. 1973 Studies of the influence of density on jet noise. *J. Sound Vib.* **28**, 649–668.
- HUGO, R. J. & McMACKIN, L. 1997 Non-intrusive linearized stability experiments on a heated axisymmetric jet. *AIAA Paper* 1997-1965.
- LAU, J. C. 1981 Effects of exit Mach number and temperature on mean-flow and turbulence characteristics in round jets. *J. Fluid Mech.* **105**, 193–218.
- LEPICOVSKY, J., AHUJA, K. K., BROWN, W. H., SALIKUDDIN, M. & MORRIS, P. J. 1988 Acoustically excited heated jets, Part III: Mean flow data. *NASA CR 4129*.
- LILLEY, G. M. 1991 Jet noise classical theory and experiments. *Aeroacoustics of Flight Vehicles: Theory and Practice*, Vol. I. *Noise Sources* (ed. H. H. Hubbard). *NASA RP 1258*.
- MICHALKE, A. & MICHEL, U. 1979 Prediction of jet noise in flight from static tests. *J. Sound Vib.* **67**, 341–367.
- MONKEWITZ, P. A., BECHERT, D. W., BARSIKOW, B. & LEHMANN, B. 1990 Self excited oscillations and mixing in a heated round jet. *J. Fluid Mech.* **213**, 611–639.
- MOREL, T. 1975 Comprehensive design of axisymmetric wind tunnel contractions. *ASME Paper* 75 FE-17.
- MORFEY, C. L. 1973 Amplification of aerodynamic noise by convected flow inhomogeneities. *J. Sound Vib.* **31**, 391–397.
- MORFEY, C. L., SZEWCZYK, V. M. & TESTER, B. J. 1978 New scaling laws for hot and cold jet mixing noise based on a geometric acoustics model. *J. Sound Vib.* **61**, 255–292.
- ÖTÜGEN, M. V. & NÄMER I. 1988 Rayleigh scattering temperature measurements in a plane turbulent air jet at moderate Reynolds numbers. *Exps. Fluids* **6**, 461–466.
- PANDA, J. & SEASHOLTZ, R. G. 2002 Experimental investigation of density fluctuations in high speed jets and correlation with generated noise. *J. Fluid Mech.* **450**, 97–130.
- PANDA, J., SEASHOLTZ, R. G., MIELKE, A. F., ELAM, K. A. & ECK, D. G. 2004 Effect of heating on turbulent density fluctuations and noise generation from high speed jets. *AIAA Paper* 2004-3016.
- PANDA, J., SEASHOLTZ, R. G. & ELAM, K. A. 2005 Investigation of noise sources in high-speed jets via correlation measurements. *J. Fluid Mech.* **537**, 349–385.
- RUSS, S. & STRYKOWSKI, P. J. 1993 Turbulent structure and entrainment in heated jets: the effect of initial conditions. *Phys. Fluids A: Fluid Dyn.* **5**, 3216–3225.
- TAM, C. K. W. & AURIULT, L. 1999 Jet mixing noise from fine scale turbulence. *AIAA J.* **37**, 145–153.
- TAM, C. K. W., GOLEBIOWSKI, M. & SEINER, J. M. 1996 On the two components of turbulent mixing noise from supersonic jets. *AIAA Paper* 96-1716.
- TANNA, H. K. 1977 An experimental study of jet noise, Part I: Turbulent mixing noise. *J. Sound Vib.* **50**, 405–428.

- TANNA, H. K., DEAN, P. T. & BURRIN, R. H. 1976 The generation and radiation of supersonic jet noise, vol. 3, Turbulent Mixing Noise Data. *Air Force Aero-Propulsion Laboratory Report AFAPL-TR-65*.
- VISWANATHAN, K. 2004 Aeroacoustics of hot jets. *J. Fluid Mech.* **516**, 39–82.
- VISWANATHAN, K. 2006 Scaling laws and a method for identifying components of jet noise. *AIAA J.* **44**, 2274–2285.
- VISWANATHAN, K. & CLARK, L. T. 2004 Effect of nozzle internal contour on jet aeroacoustics. *Intl J. Aeroacoust.* **3**, 103–135.
- WHITE, F. M. 1973 *Viscous Fluid Flow*. McGraw-Hill.